Atmos. Meas. Tech. Discuss., 8, 8727–8752, 2015
www.atmos-meas-tech-discuss.net/8/8727/2015/
doi:10.5194/amtd-8-8727-2015

Atmospheric Measurement Techniques Discussions

Implications of MODIS bowtie distortion on aerosol optical depth retrievals, and techniques for mitigation

A. M. Sayer[1,2], **N. C. Hsu**[1], **and C. Bettenhausen**[1,3]

[1]NASA Goddard Space Flight Center, Greenbelt, Maryland, USA
[2]Goddard Earth Sciences Technology And Research (GESTAR), Universities Space Research Association (USRA), Columbia, Maryland, USA
[3]Science Systems and Applications Inc., Lanham, Maryland, USA

Received: 20 July 2015 – Accepted: 4 August 2015 – Published: 18 August 2015

Correspondence to: A. M. Sayer (andrew.sayer@nasa.gov)

Published by Copernicus Publications on behalf of the European Geosciences Union.

Abstract

The scan geometry of the Moderate Resolution Imaging Spectroradiometer (MODIS) sensors results in a pixel shape distortion known as the "bowtie effect". Specifically, sensor pixels near the edge of the swath are elongated along-track and across-track compared to pixels near the centre of the swath, resulting in an increase of pixel area by up to a factor of ~ 9, and additionally pixels acquired from consecutive scans overlap. The Deep Blue and Dark Target aerosol optical depth (AOD) retrieval algorithms aggregate sensor pixels and provide level 2 (L2) AOD at a nominal horizontal pixel size of 10 km, but the bowtie distortion means that they also suffer from this size increase and overlap. This means that the spatial characteristics of the data vary as a function of satellite viewing zenith angle (VZA) and, for VZA > 30°, corresponding to approximately 50 % of the data, are areally enlarged by a factor of 50 % or more compared to this nominal pixel area, and are not spatially independent of each other. This has implications for retrieval uncertainty and aggregated statistics, causing a narrowing of AOD distributions near the edge of the swath, as well as for data comparability from the application of similar algorithms to sensors without this level of bowtie distortion. Additionally, the pixel overlap is not obvious to users of the L2 aerosol products because only pixel centres, not boundaries, are provided within the L2 products. A two-step procedure is proposed to mitigate the effects of this distortion on the MODIS aerosol products. The first (simple) step involves changing the order in which pixels are aggregated in L2 processing to reflect geographical location rather than scan order, which removes the bulk of the overlap between L2 pixels, and slows the rate of growth of L2 pixel size vs. VZA. This can be achieved without significant changes to existing MODIS processing algorithms. The second step involves additionally changing the number of sensor pixels aggregated across-track as a function of VZA, which preserves L2 pixel size at around 10 km × 10 km across the whole swath, but would require algorithmic quality assurance tests to be re-evaluated. Both of these steps also improve the extent to which

AMTD
8, 8727–8752, 2015

the pixel locations a user would infer from the L2 data products represent the actual spatial extent of the L2 pixels.

1 Introduction

The Moderate Resolution Imaging Spectroradiometers (MODIS) aboard the Terra and Aqua platforms have been used to create data products for a range of Earth science disciplines, including analyses of the atmospheric aerosol burden. Midvisible aerosol optical depth (AOD) data products have been generated routinely by a variety of dedicated algorithms over bright (Hsu et al., 2004, 2006, 2013) and dark (Kaufman et al., 1997; Levy et al., 2007, 2013; Hsu et al., 2013) land surfaces, ocean surfaces (Tanré et al., 1997; Levy et al., 2013), and as a by-product of algorithms for the atmospheric correction of land/ocean surface reflectance (e.g. Ahmad et al., 2010; Lyapustin et al., 2011).

The level 2 (L2, orbit-level) MODIS dedicated aerosol product data product is known as MOD04 for data generated from MODIS Terra, and MYD04 for data from MODIS Aqua (hereafter MXD04 collectively). The latest version of MXD04 products (Collection 6, C6) contains data generated by the Deep Blue (DB) algorithms over land surfaces (Hsu et al., 2013), a Dark Target (DT) over-land algorithm, and an over-water algorithm which also uses wavelengths at which the water surface is dark (Levy et al., 2013). These L2 products are generated from level 1b (L1b) calibrated radiance data measured by the MODIS instruments. To decrease noise in the retrieval and provide a manageable data volume, the standard L2 products are provided at a nominal horizontal pixel size of 10 km (referred to as "retrieval pixels"), compared to a L1b pixel size of 0.25–1 km (dependent on band, referred to as "sensor pixels"). As aerosol horizontal variations are often on length scales of order tens of km (e.g. Anderson et al., 2003), this pixel size should preserve the underlying spatial shape of aerosol fields without major smoothing of features. Note that a separate nominal 3 km DT product is also

AMTD
8, 8727–8752, 2015

available, albeit with larger uncertainties than the 10 km standard product (Munchak et al., 2013; Remer et al., 2013, Livingston et al., 2014).

However, a consequence of the MODIS scan geometry, of which many users of MXD04 data may not be aware, is a distortion of pixel size and shape from the center to the edge of the swath. This is known as the "bowtie effect" and has the potential to alias into angle-dependent artefacts and changes in retrieval quality in the derived data sets. It also presents a challenge for the continuation of MODIS-like data sets using similar sensors such as the Visible Infrared Imaging Radiometer Suite (VIIRS) on the Suomi National Polar-orbiting Partnership (S-NPP) platform, launched in late 2011, for which these bowtie distortions are much smaller. Consequently, data sets generated from similar algorithms may exhibit different angular-dependent characteristics.

The purpose of this study is to illustrate the influence of the MODIS bowtie distortion on AOD retrievals, and examine some techniques for mitigation of these distortions, for potential application in future MODIS (or VIIRS) data reprocessings. Section 2 discusses MODIS and its scan geometry, providing an illustration of the bowtie effect and the dependence of MODIS AOD retrievals on view angle. Section 3 proposes a two-step solution to mitigate these effects, of which the first step is relatively simple and could be accomplished with minor changes to existing MODIS processing algorithms, while the second step would require more careful evaluation. Finally, Sect. 4 provides a discussion on the importance of the results.

2 Illustration of the problem

MODIS takes measurements in a total of 36 bands with central wavelengths between 412 nm and 14.4 µm (Barnes et al., 1998; Toller et al., 2013). The L1b data are organised into 5 min granules, which consist of 1354 pixels across-track and 203 scans along-track. The term "along-track" indicates the direction of the satellite flight track (for daytime data this is approximately from North to South for Terra, and from South to North for Aqua, due to the satellites' $\sim 98.2^{\circ}$ inclination), while "across-track" indicates

AMTD
8, 8727–8752, 2015

the direction perpendicular to the flight track (alternating East-West and West-East for successive scans). This is illustrated in Fig. 1.

Each scan is approximately 10 km wide at nadir; for nominal 1 km bands, there are 10 detectors; 20 detectors for 0.5 km bands, and 40 detectors for the two bands at nominal 0.25 km resolution. In the L1b products, the data are available both at native resolution, and aggregated to the footprints of the coarser bands. For example MODIS bands 1 and 2, centred near 650 and 860 nm respectively, are recorded with a nominal 0.25 km pixel size; however, they are additionally provided aggregated to the footprints of the 0.5 km bands (which is native resolution for bands 3–7) and 1 km bands (which is native resolution for bands 8–36). DB uses the L1b data aggregated to 1 km while the DT algorithms use the L1b data at 0.5 km.

The L2 aerosol products are created by aggregating blocks of contiguous sensor pixels through one scan along-track, and 10 1 km sensor pixels across-track (or 20 0.5 km pixels for the appropriate bands in DT). The DB algorithms (Hsu et al., 2013) retrieve AOD from suitable (e.g. cloud-free snow-free) data at sensor pixel resolution and then aggregate to retrieval pixel resolution (a "retrieve-then-average" technique), while the DT algorithms (Levy et al., 2013) average measured radiance from suitable pixels and then perform a single retrieval at retrieval pixel resolution (an "average-then-retrieve" technique). The two averaging methods should be equivalent if the underlying scene is homogeneous, but not if there is surface or atmospheric heterogeneity. Thus, the L2 aerosol products consist of 135 retrieval positions across-track and 203 along-track (the four excess across-track positions are discarded as 1354 does not divide evenly by 10). As the sensor scans across-track back and forth, the light observed by MODIS is reflected from a scan mirror onto the focal plane assemblies. Dependent on the scan direction, both sides of this scan mirror are used. Differences in the quality of the characterisation of these two mirror sides can lead to striping in the data between forward and reverse scans in some situations (Franz et al., 2007).

Because of this scan geometry the spatial resolution degrades from nadir (viewing zenith angle, VZA 0°) to the scan edge (VZA ~ 65°), such that pixels near the edge of

AMTD
8, 8727–8752, 2015

the scan are larger than those near nadir; the swath width is ~ 2330 km, despite the fact that there are only 1354 across-track positions. The primary distortion is across-track (i.e. pixels get longer in the longitudinal direction) but there is also an along-track (i.e. latitudinal) distortion, resulting in overlap between pixels from consecutive scans near the swath edges. These give a scan a shape similar to a bow tie, hence the term "bowtie effect".

These effects are illustrated for an example MODIS Terra granule in Figs. 2 and 3. This granule is the basis for most of the results shown in this study. Note that slight asymmetries and discontinuities in the retrieval pixel size result because of variations in terrain elevation across the granule. Although the nominal 10 km × 10 km horizontal resolution results in a retrieval pixel area of ~ 100 km^2 near the centre of the swath, as the VZA increases, the pixel area is increased by almost a factor of 10 at the extreme edges of the swath. Figure 3 shows that the median absolute VZA is about 30°, for which pixel area is increased by around ~ 50 % compared with VZA = 0°. Hence, although the MODIS aerosol retrieval pixel size is commonly stated to be 10 km × 10 km, half the time the actual area encompassed by these retrieval pixels is at least 50 % larger than that. Note that the sign of VZA in Fig. 3 is defined such that positive values are found on the western side of the swath.

Taking a closer view of the area near the western edge of the swath, Fig. 4 shows the ground locations of the sensor and retrieval pixels. Scans are coloured alternating in red and blue (odd scans in red, even in blue). Two factors are immediately apparent. One is the strong elongation of pixels in the across-track (longitudinal) direction. The second is that, at the swath edge, successive scans (e.g. a red-coloured scan and the blue-coloured scans immediately before and after it) are fully overlapped in the along-track direction. Each edge-of-swath retrieval covers half of the area of the retrieval pixel from the scan before it, and half of the area from the scan after it. Even ten retrievals in from the scan edge the retrieval pixels are more than half overlapped between successive scans. This therefore represents a sizeable fraction of the MXD04 data, particularly in terms of area covered.

AMTD
8, 8727–8752, 2015

This overlap is not obvious to L2 data product users, as the L2 files only present the central latitudes and longitudes for the retrieval pixels. Figure 5 shows the same retrieval pixel locations as in Fig. 4, except with the retrieval pixel boundaries which would be inferred from the L2 central latitudes/longitudes overplotted. Thus, the oversampling and overlap of the L2 data is not clear if the L2 data are mapped without auxiliary knowledge of the L1b sensor pixel locations.

All other things being equal, the expected effects of both aspects of this distortion (i.e. pixel enlargement and overlap) on the MXD04 products would be to decrease the variability of the retrieved AOD near the edge of the scan compared to that near the centre of the scan. Figure 6 shows histograms of AOD at 550 nm from all four algorithm/surface types included within the C6 MXD04 products (DB over arid and vegetated surfaces; DT over land and ocean), for data with VZA $< 10^{\circ}$ and VZA $> 55^{\circ}$, corresponding to roughly the lowest and highest VZA quintiles respectively (Fig. 3). These histograms are calculated from all L2 products for the year 2006; for the DT ocean panel only latitudes poleward of 35° are used, as otherwise a sampling bias may be introduced due to the presence of Sun glint near the centre of the swath in tropical regions.

The median, standard deviations, and width of the central 68 % of the data (i.e. difference between 86th and 14th percentiles of AOD) for these histograms are shown in Table 1. In all cases, the retrievals near the edge of the swath show smaller variability than those near the centre, which is consistent with the expected effects of the bowtie distortion. The median AOD is more stable between the two sets of VZA. The decrease in variability (~ 25 % decrease in AOD standard deviation or width of central 68 %) is most pronounced for the dark (vegetated) land surfaces in DB and DT. This may reflect the lack of strong aerosol point sources over the open ocean, and potentially the spatial scales of aerosol features over desert and ocean surfaces being larger than aerosols over vegetated land.

Note that the differences between DB and DT histogram shapes over dark vegetated surfaces are due in part to algorithmic assumptions; for example, what surface counts

AMTD
8, 8727–8752, 2015

as dark vs. bright in the two algorithms, and the fact that DT over land allows retrievals of small negative AOD (down to −0.05) while DB does not. All histogram shapes may also be influenced by the fact that the algorithms' AOD retrieval uncertainties can be a factor of solar and viewing geometry (e.g. Hyer et al., 2011; Sayer et al., 2013, 2014). However Table 1 and Fig. 6 support the assertion that the retrieval overlap and size distortion, undesirable from a point of view of homogeneity of data characteristics, may also be influencing the statistics of the retrieved AOD.

3 Potential mitigation techniques

3.1 Reordering along-track sensor pixel aggregation

The most straightforward way to ameliorate the effects of the bowtie distortion on the MXD04 aerosol products would simply be to change the along-track sensor pixel aggregation order from one based on the order of data collection (i.e. scan order) to one based on the order in which pixel centres are arranged on the ground (i.e. geographical order). This could be achieved by reordering the L1b data at each across-track position within each granule in order of increasing (for Aqua) or decreasing (for Terra) latitude, and would not require any other changes to data processing algorithms or output data file format. This is referred to hereafter as the "resorted" aggregation technique, and has the basic effect of decreasing the distortion in the along-track direction.

A comparison between swath-edge L2 standard and resorted retrieval pixel boundaries is shown in Fig. 7. The 100 % areal overlap of swath-edge pixels in the standard aggregation is reduced to around 40 % in the resorted aggregation, and effectively removed by a distance of a half-dozen retrieval pixels in to the swath (while in the standard aggregation pixels are still significantly overlapped at this position). Additionally, although the spatial overlap is ∼ 40 %, the overlap in terms of L1b pixel radiance data is only ∼ 20 %, as the central (non-overlapped) 60 % of the resorted retrieval pixel contains data from 8 out of the 10 along-track positions within the cell. This resorting

AMTD
8, 8727–8752, 2015

technique also means that the actual area covered by each pixel now aligns much more closely with the area that a data user would infer based on the geolocation information within the L2 data products (cf. Fig. 5).

Because of the DB retrieve-then-average methodology, it is most straightforward to use the DB algorithm to illustrate the effects of changing the aggregation technique on AOD retrievals than DT. Figure 8 shows the difference in AOD and pixel area for this technique as compared to the standard L2 aggregation (Fig. 2). The large-scale AOD patterns do not change, although some striping is reduced (as pixels from scans using both mirror sides are now included in the same retrieval pixel, mitigating residual calibration effects on AOD discontinuities). The median AOD difference is, as expected, negligible (< 0.01) and the standard deviation of the AOD difference is 0.02. The main advantage from this approach, however, is the reduction of retrieval pixel area by up to around 40 % (Fig. 8d) at the edge of scan compared to the standard aggregation, due to the removal of much of the along-track retrieval pixel growth and overlap. For VZA $> 30^{\circ}$, the increase of pixel area with VZA proceeds only about half as quickly, for a factor of around 5 at the edge of the scan, compared to around a factor of 9 using the standard aggregation.

3.2 Change of across-track pixel aggregation counts

Although the resorting technique described in Sect. 3.1 increases retrieval pixel independence and decreases pixel size by addressing the along-track aspect of the bowtie distortion, it does not improve the across-track pixel growth vs. VZA, which is the larger of the two contributions to retrieval pixel size increase. In an ideal situation retrieval pixel size and shape would not vary with across-track scan position, but for MODIS this can only be accomplished by changing the number of pixels aggregated across-track when going from sensor pixel to L2 retrieval pixel resolution.

This has larger potential implications for the MXD04 product than only performing the resorting aggregation, because quality assurance (QA) procedures used to identify L2 retrievals suitable for quantitative analysis (Hsu et al., 2013; Levy et al., 2013) de-

AMTD
8, 8727–8752, 2015

pend on the statistics of the data within the L2 retrieval pixel, including the number of available sensor pixels for retrieval, and additionally because the size of the resulting L2 data arrays would change, which may affect some data users. Thus it is likely that changing the across-track pixel aggregation (in addition to applying the resorting technique of Sect. 3.1 to mitigate along-track distortion) would change the error characteristics of the MXD04 products more significantly, and require more careful assessment prior to large-scale implementation.

The combination of resorting along-track and changing across-track aggregation number is referred to hereafter as the "variable aggregation" technique. Figure 9 shows that by changing the number of across-track positions aggregated as a function of VZA, from 2 near the edge of the swath to 10 (as in the standard MXD04 aggregation) near the centre, it is possible to preserve an pixel area of around 100 km^2 across the whole MODIS swath. This results in an increase of L2 data array size from 203 × 134 retrieval pixels to 203 × 233 retrieval pixels. Note that 10 pixels are still aggregated along-track, so near the edge of the swath a total of 20 L1b sensor pixels would contribute to the L2 retrieval pixel, while for VZA smaller than $\sim 10^{\circ}$ the aggregation remains the same as in the standard product (i.e. 100 sensor pixels per L2 pixel). One further point of relevance, however, is that since the source L1b sensor pixels are still distorted, and the atmospheric path length is also dependent on VZA, it is still possible that the error characteristics of the retrievals, and efficacy of cloud tests making use of spatial homogeneity (e.g. Martins et al., 2002), could change as a function of VZA.

Because of the preservation of horizontal pixel size vs. VZA, the variable aggregation technique has larger implications for the spatial distribution of retrieved AOD than the resorted technique (Sect. 3.1). Figure 10 shows part of the eastern edge of the granule from Fig. 2, comparing the spatial distributions of AOD for each aggregation method. Note that the retrieval pixels are drawn here corresponding to their locations which would be inferred from the L2 geolocation information. The standard and resorted methods show similar spatial features; the decrease in striping from the resorted aggregation is obvious. The variable aggregation technique reveals the struc-

AMTD
8, 8727–8752, 2015

ture of the visible dust plumes with much better fidelity. Data holes are also much more closely aligned with the presence of clouds; while this will not affect the L2 retrievals themselves (as only cloud-free sensor pixels are used), it does improve the utility of the data for those wishing to assess the dependence of aerosol properties as a function of distance from clouds (e.g. Bar-Or et al., 2011; Várnai et al., 2013), or collocate aerosol and cloud data for other purposes.

4 Perspectives on product regularity and MODIS/VIIRS continuity

The full influence of the MODIS bowtie effect on the MXD04 aerosol data products has not received wide recognition up to this point. Although visualisations of the data make the elongation of L2 pixels fairly obvious, the substantial overlap between them at the edge of the swath, and the effect that this oversampling and enlargement may have on the L2 data and aggregated statistics, has been underappreciated, and many data users may be unaware of it because it cannot be inferred from the L2 data products in isolation.

Although this distortion has not hindered the widespread use of the MXD04 data products for scientific applications, the issue is increasingly relevant now that MODIS-like algorithms are being developed for application to NPP-VIIRS data. The VIIRS sensor makes measurements at similar spectral bands to MODIS, with a similar L1b sensor pixel size of nominal 0.75 km for moderate-resolution bands (M-bands), and a broader swath (3040 km). VIIRS has a similar across-track scanning pattern to MODIS, although with 16 M-band detectors per scan. However, VIIRS incorporates several design features to reduce the bowtie distortion (Wolfe et al., 2012). Firstly, the VIIRS on-board native pixel size is actually smaller than the nominal M-band size in the across-track direction. The scan is divided into three regions (in both directions). From nadir out to a scan angle of 31.72°, three pixels are aggregated across-track to create the M-band L1b data; from 31.72–44.86° two pixels are aggregated, and from 44.86° to the edge of scan no aggregation is performed. Additionally, at the outer two aggregation zones,

AMTD
8, 8727–8752, 2015

two and four pixels respectively are deleted from the along-track scan edges (so-called "bowtie deletion"). The net effect of this is that pixels within each aggregation zone are enlarged in length by at most approximately only a factor of two, and that overlap between sensor pixels from consecutive scans is in most cases two or fewer detectors, compared to up to 100 % in MODIS. Thus, there are structural reasons that, even if the AOD retrieval algorithms are as close as possible, the characteristics of L2 data derived from the sensors may differ, which has implications for MODIS/VIIRS data continuity and the generation of multi-sensor long-term climate data records.

It is therefore recommended that future reprocessings of the MODIS aerosol data records consider ways to mitigate the effect of the bowtie distortion on the spatial structure of the AOD products. In the meantime this study is intended to serve as a point of reference to bring these issues to wider recognition within the data user community. Aggregating sensor pixels by geographical location rather than in along-track scan order is one straightforward step which can be taken to decrease the along-track distortion, however, as discussed, taking the additional step of changing to a variable across-track aggregation has larger implications for algorithm development and QA tests. This is already an issue which algorithm developers are facing to an extent, because with the VIIRS bowtie deletion the number of valid sensor pixels also changes as a function of VZA through the three M-band aggregation zones.

Although presented here in the context of the DB and DT AOD retrieval algorithms, these types of issues will be common to any algorithm which aggregates MODIS data to a coarser resolution. The mitigation is fairly straightforward for this example because the MXD04 spatial resolution matches the along-track length of one scan (i.e. 10 nominal 1 km sensor pixels). However for data products where the L2 resolution does not match the scan length, such as the DT nominal 3 km AOD product (Remer et al., 2013), the distortion will have an irregular impact on the actual and perceived size of the L2 retrieval pixels. Thus, to obtain a L2 product where the pixel-to-pixel variation in area covered is minimised, it makes most sense to perform retrievals at either the coarsest L1b data pixel size (i.e. nominal 1 km for MODIS or 0.75 km for VIIRS) or else with an

AMTD
8, 8727–8752, 2015

along-track aggregation which is an exact divisor (or multiple) of the scan length (e.g. 5 or 10 km for MODIS; 3, 6, or 12 km for VIIRS).

Acknowledgements. This work was supported by the NASA EOS program, managed by H. Maring. The MODIS Characterization Support Team and Ocean Biology Processing Group are thanked for their extensive efforts in maintaining the high radiometric quality of MODIS data. MODIS level 1 data and aerosol products are available from http://ladsweb.nascom.nasa.gov.

References

Ahmad, Z., Franz, B. A., McClain, C. R., Kwiatowska, E. J., Werdell, J., Shettle, E. P., and Holben, B. N.: New aerosol models for the retrieval of aerosol optical thickness and normalized water-leaving radiances from the SeaWiFS and MODIS sensors over coastal regions and open oceans, Appl. Optics, 49, 5545–5560, doi:10.1364/AO.49.005545, 2010. 8729

Anderson, T. L., Charlson, R. J., Winker, D. M., Ogren, J. A., and Holmén, K.: Mesoscale Variations of Tropospheric Aerosols, J. Atmos. Sci., 60, 119–136, doi:10.1175/1520-0469(2003)060<0119:MVOTA>2.0.CO;2, 2003. 8729

Bar-Or, R. Z., Altaratz, O., and Koren, I.: Global analysis of cloud field coverage and radiative properties, using morphological methods and MODIS observations, Atmos. Chem. Phys., 11, 191–200, doi:10.5194/acp-11-191-2011, 2011. 8737

Barnes, W. L., Pagano, T. S., and Salomonson, V. V.: Prelaunch characteristics of the Moderate Resolution Imaging Spectroradiometer (MODIS) on EOS-AM1, IEEE T. Geosci. Remote, 36, 1088–1100, doi:10.1109/36.700993, 1998. 8730

Franz, B. A., Kwiatkowska, E. J., Meister, G., and McClain, C. R.: Utility of MODIS-Terra for ocean color applications, P. SPIE IS&T Elect. Im., 6677, doi:10.1117/12.732082, 2007. 8731

Hsu, N. C., Tsay, S.-C., King, M. D., and Herman, J. R.: Aerosol properties over bright-reflecting source regions, IEEE T. Geosci. Remote, 42, 557–569, doi:10.1109/TGRS.2004.824067, 2004. 8729

Hsu, N. C., Tsay, S.-C., King, M. D., and Herman, J. R.: Deep Blue retrievals of Asian aerosol properties during ACE-Asia, IEEE T. Geosci. Remote, 44, 3180–3195, doi:10.1109/TGRS.2006.879540, 2006. 8729

AMTD
8, 8727–8752, 2015

Hsu, N. C., Jeong, M.-J., Bettenhausen, C., Sayer, A. M., Hansell, R., Seftor, C. S., Huang, J., and Tsay, S.-C.: Enhanced deep blue aerosol retrieval algorithm: the second generation, J. Geophys. Res., 118, 9296–9315, doi:10.1002/jgrd.50712, 2013. 8729, 8731, 8735

Hyer, E. J., Reid, J. S., and Zhang, J.: An over-land aerosol optical depth data set for data assimilation by filtering, correction, and aggregation of MODIS Collection 5 optical depth retrievals, Atmos. Meas. Tech., 4, 379–408, doi:10.5194/amt-4-379-2011, 2011. 8734

Kaufman, Y. J., Wald, A. E., Remer, L. A., Gao, B.-C., Li, R.-R., and Flynn, L.: The MODIS 2.1 µm channel-correlation with visible reflectance for use in remote sensing of aerosol, IEEE T. Geosci. Remote, 35, 1286–1298, doi:10.1109/36.628795, 1997. 8729

Levy, R. C., Remer, L. A., Mattoo, S., Vermote, E. F., and Kaufman, Y. J.: Second-generation operational algorithm: retrieval of aerosol properties over land from inversion of Moderate Resolution Imaging Spectroradiometer spectral reflectance, J. Geophys. Res., 112, D13211, doi:10.1029/2006JD007811, 2007. 8729

Levy, R. C., Mattoo, S., Munchak, L. A., Remer, L. A., Sayer, A. M., Patadia, F., and Hsu, N. C.: The Collection 6 MODIS aerosol products over land and ocean, Atmos. Meas. Tech., 6, 2989–3034, doi:10.5194/amt-6-2989-2013, 2013. 8729, 8731, 8735

Livingston, J. M., Redemann, J., Shinozuka, Y., Johnson, R., Russell, P. B., Zhang, Q., Mattoo, S., Remer, L., Levy, R., Munchak, L., and Ramachandran, S.: Comparison of MODIS 3 km and 10 km resolution aerosol optical depth retrievals over land with airborne sunphotometer measurements during ARCTAS summer 2008, Atmos. Chem. Phys., 14, 2015–2038, doi:10.5194/acp-14-2015-2014, 2014. 8730

Lyapustin, A., Wang, Y., Laszlo, I., Kahn, R., Korkin, S., Remer, L., Levy, R., and Reid, J. S.: Multiangle implementation of atmospheric correction (MAIAC): 2. Aerosol algorithm, J. Geophys. Res., 116, D03211, doi:10.1029/2010JD014986, 2011. 8729

Martins, J. V., Tanré, D., Remer, L., Kaufman, Y., Mattoo, S., and Levy, R.: MODIS Cloud screening for remote sensing of aerosols over oceans using spatial variability, Geophys. Res. Lett., 29, 1619, doi:10.1029/2001GL013252, 2002. 8736

Munchak, L. A., Levy, R. C., Mattoo, S., Remer, L. A., Holben, B. N., Schafer, J. S., Hostetler, C. A., and Ferrare, R. A.: MODIS 3 km aerosol product: applications over land in an urban/suburban region, Atmos. Meas. Tech., 6, 1747–1759, doi:10.5194/amt-6-1747-2013, 2013. 8730

AMTD
8, 8727–8752, 2015

Remer, L. A., Mattoo, S., Levy, R. C., and Munchak, L. A.: MODIS 3 km aerosol product: algorithm and global perspective, Atmos. Meas. Tech., 6, 1829–1844, doi:10.5194/amt-6-1829-2013, 2013. 8730, 8738

Sayer, A. M., Hsu, N. C., Bettenhausen, C., and Jeong, M.-J.: Validation and uncertainty estimates for MODIS Collection 6 "Deep Blue" aerosol data, J. Geophys. Res., 118, 7864–7872, doi:10.1002/jgrd.50600, 2013. 8734

Sayer, A. M., Munchak, L. A., Hsu, N. C., Levy, R. C., Bettenhausen, C., and Jeong, M.-J.: MODIS Collection 6 aerosol products: comparison between Aqua's e-Deep Blue, Dark Target, and "merged" data sets, and usage recommendations, J. Geophys. Res., 119, 13965–13989, doi:10.1002/2014JD022453, 2014. 8734

Tanré, D., Kaufman, Y. J., Herman, M., and Mattoo, S.: Remote sensing of aerosol properties over oceans using the MODIS/EOS spectral radiances, J. Geophys. Res., 102, 16971–16988, doi:10.1029/96JD03437, 1997. 8729

Toller, G., Xiong, X., Sun, J., Wenny, B. N., Geng, X., Kuyper, J., Angal, A., Chen, H., Madhavan, S., and Wu, A.: Terra and aqua moderate-resolution imaging spectroradiometer collection 6 level 1B algorithm, J. Appl. Remote Sens., 7, 073557, doi:10.1117/1.JRS.7.073557, 2013. 8730

Várnai, T., Marshak, A., and Yang, W.: Multi-satellite aerosol observations in the vicinity of clouds, Atmos. Chem. Phys., 13, 3899–3908, doi:10.5194/acp-13-3899-2013, 2013. 8737

Wolfe, R. E., Lin, G., Nishihama, M., Tewari, K. P., and Montano, E.: NPP VIIRS early on-orbit geometric performance, P. SPIE IS&T Elect. Im., 8510, doi:10.1117/12.929925, 2012. 8737

AMTD
8, 8727–8752, 2015

Table 1. Median, standard deviation, and width of central 68 % of AOD at 550 nm for the histograms shown in Fig. 6.

Algorithm	VZA range	Median AOD	Standard deviation of AOD	Width of central 68 %
DB arid	< 10°	0.14	0.30	0.38
	> 55°	0.15	0.29	0.35
DB vegetated	< 10°	0.09	0.15	0.21
	> 55°	0.06	0.11	0.14
DT vegetated	< 10°	0.05	0.18	0.13
	> 55°	0.05	0.15	0.09
DT ocean	< 10°	0.12	0.20	0.13
	> 55°	0.11	0.13	0.12

AMTD
8, 8727–8752, 2015

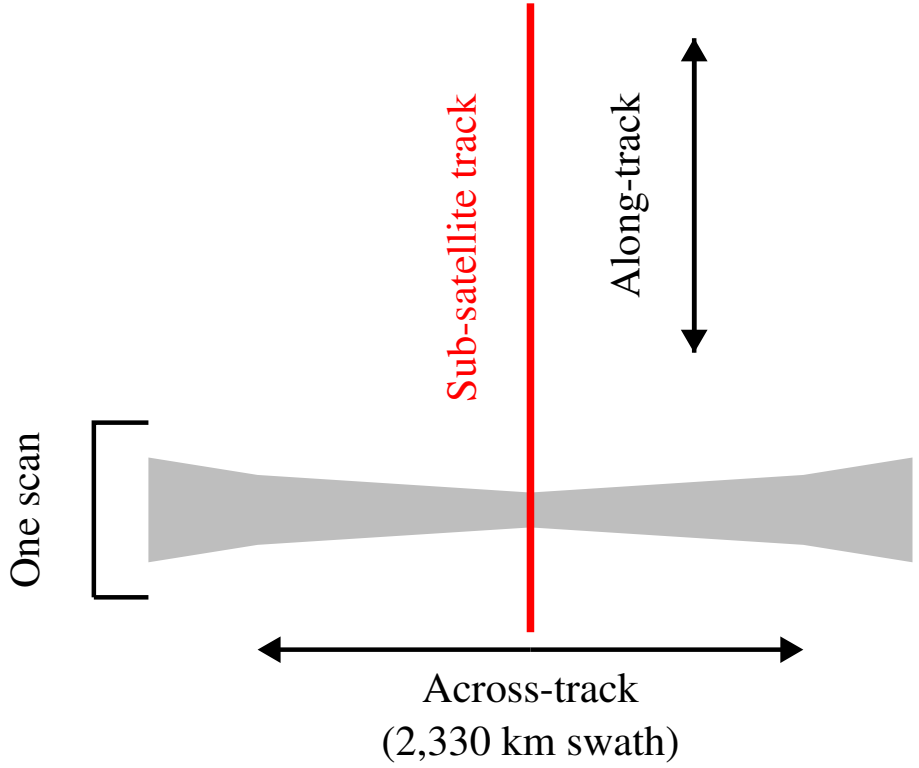

Figure 1. Illustration of some terms related to MODIS scan geometry.

AMTD
8, 8727–8752, 2015

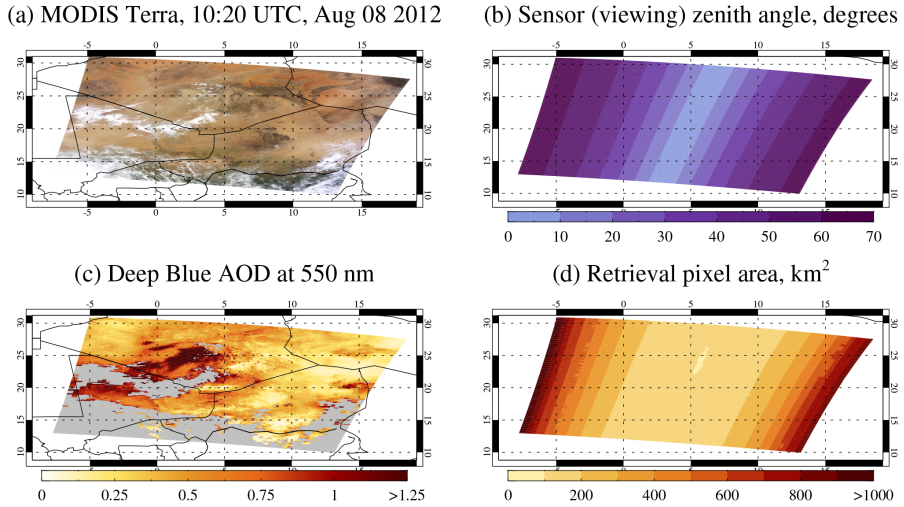

Figure 2. MODIS granule used as a case study throughout this manuscript. Panel **(a)** shows a true-colour composite, **(b)** the VZA along and across the scans, **(c)** the L2 (nominal 10 km) Deep Blue retrieved AOD for the granule, and **(d)** the Deep Blue retrieval pixel area.

AMTD
8, 8727–8752, 2015

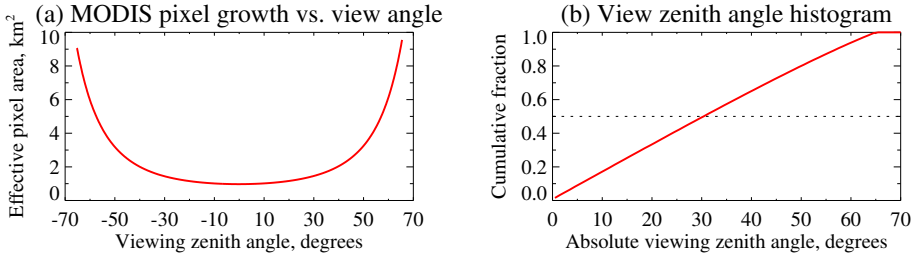

Figure 3. (a) Area of nominal 1 km × 1 km sensor pixels as a function of VZA, and **(b)** histogram of absolute VZA. The median is shown with a dashed line. Data for the MODIS granule shown in Fig. 2.

AMTD
8, 8727–8752, 2015

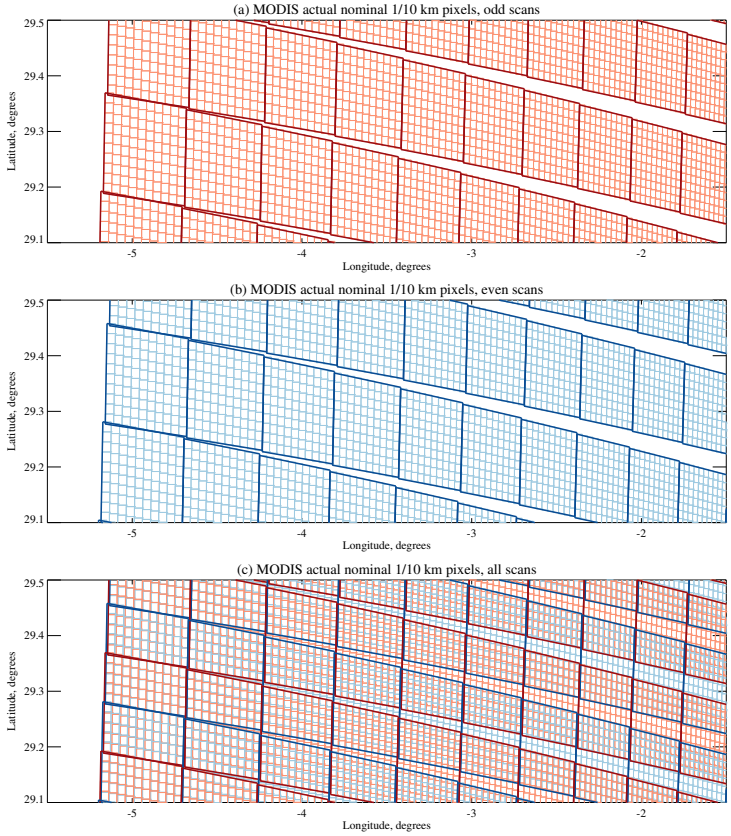

Figure 4. Borders of nominal 1 km sensor pixels (pale colours) and nominal 10 km retrieval pixels (strong colours) along the western edge of the granule shown in Fig. 2, illustrating the overlap between scans near swath edges. Data from alternating forward/backward scans are shown in red and blue. Panel **(a)** shows odd-numbered scans only, **(b)** even-numbered scans only, and **(c)** all scans.

AMTD
8, 8727–8752, 2015

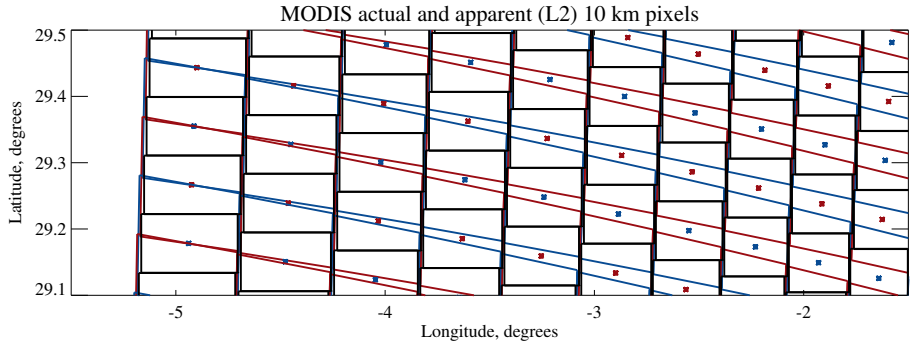

Figure 5. Borders of nominal 10 km retrieval pixels (strong colours, as in Fig. 4c) along the western edge of the granule shown in Fig. 2. Pixel centres are overplotted with coloured asterisks, and inferred L2 pixel bounds drawn in black lines.

AMTD
8, 8727–8752, 2015

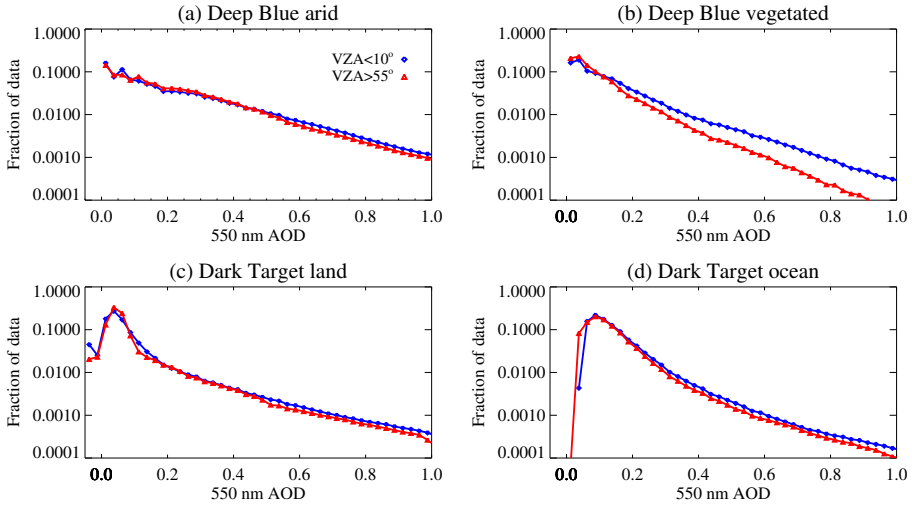

Figure 6. Histograms of retrieved MODIS Aqua AOD at 550 nm during the year 2006 retrieved from **(a)** DB over bright arid surfaces; **(b)** DB over dark vegetated surfaces; **(c)** DT over dark vegetated surfaces, and **(d)** the over-water DT algorithm.

AMTD
8, 8727–8752, 2015

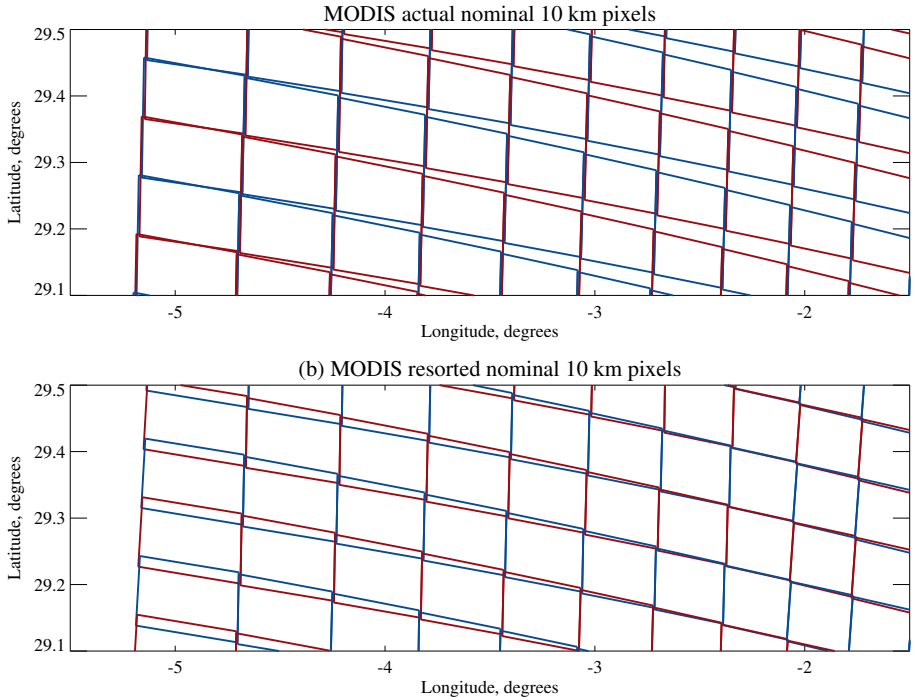

Figure 7. Actual L2 retrieval pixel boundaries for **(a)** the standard (Figs. 4c and 5) and **(b)** re-sorted aggregation techniques.

AMTD
8, 8727–8752, 2015

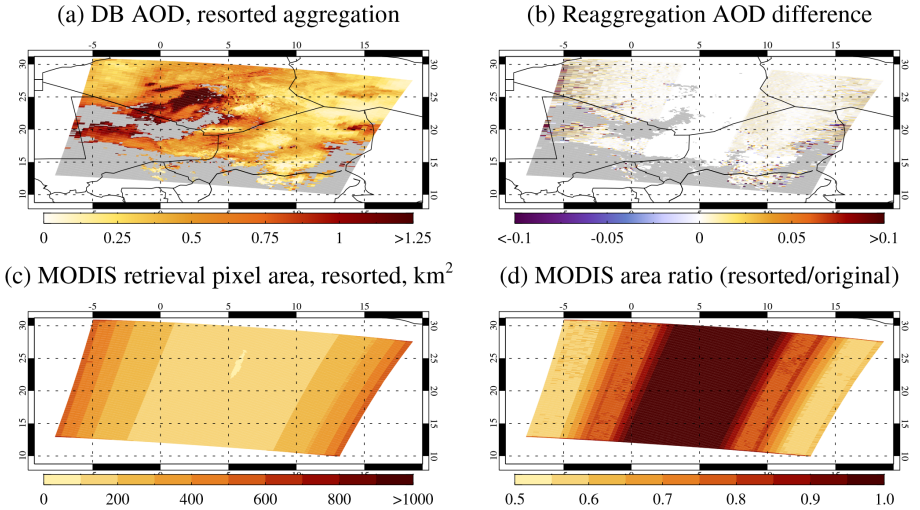

Figure 8. DB AOD retrieval for the granule in Fig. 2 using the "resorted" aggregation technique. Panel **(a)** shows the DB AOD at 550 nm, **(b)** the difference from the AOD using the standard aggregation technique (Fig. 2c), **(c)** the resulting retrieval pixel area, and **(d)** the ratio of the area using the resorted technique to that from the standard technique (i.e. ratio of panel **c** to Fig. 2d). Pixels without retrievals are shaded in grey.

AMTD
8, 8727–8752, 2015

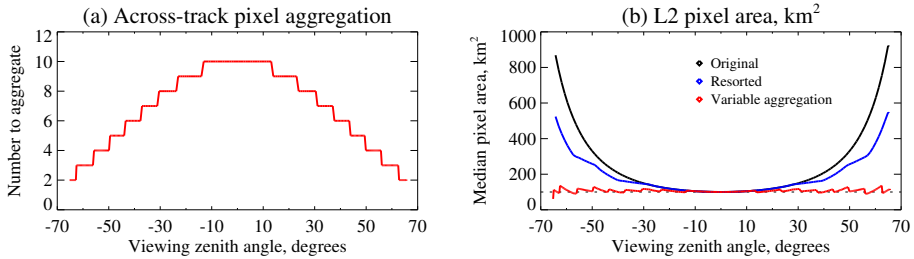

Figure 9. (a) Number of across-track positions aggregated for the "variable aggregation" technique, and **(b)** pixel area as a function of VZA for the granule shown in Fig. 2 for all three aggregation techniques. The dashed line indicates an area of 100 km^2.

AMTD
8, 8727–8752, 2015

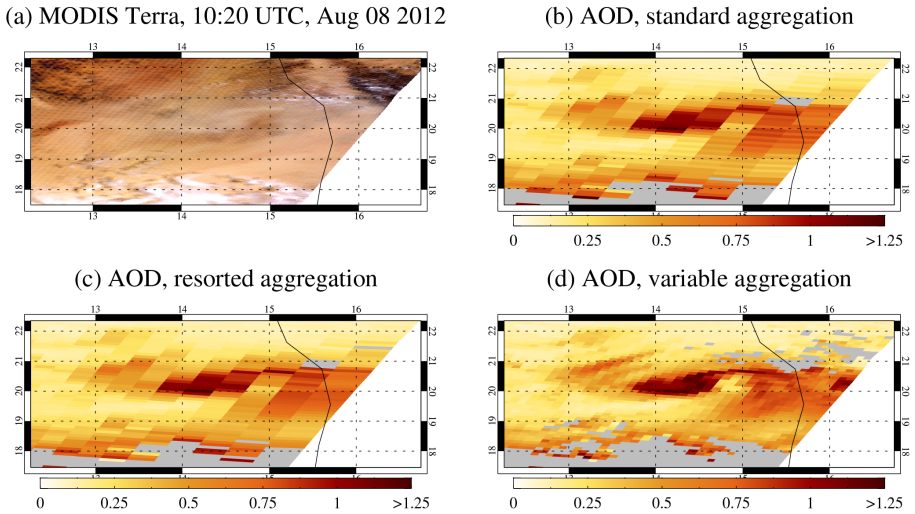

Figure 10. Effect of aggregation technique on spatial distribution of retrieved DB AOD at 550 nm. Panel **(a)** shows a true-colour image for the eastern portion of the granule shown in Fig. 2, and panels **(b–d)** show the L2 AOD for each of the standard, resorted, and variable aggregation techniques respectively. Pixels without retrievals are shaded in grey.

AMTD
8, 8727–8752, 2015